

Thermal plasma fabricated lithium niobate-tantalate films on sapphire substrate

S. A. Kulinich^{a)} and T. Yoshida

Department of Materials Engineering, Faculty of Engineering, The University of Tokyo, Hongo 7-3-1, Bunkyo-ku, Tokyo 113-8656, Japan

H. Yamamoto and K. Terashima

Department of Advanced Materials Science, Graduate School of Frontier Sciences, The University of Tokyo, Kashiwanoha 5-1-5, Kashiwa-shi, Chiba 277-8561, Japan

(Received 12 September 2002; accepted 21 April 2003; published 4 June 2003; publisher error corrected 13 June 2003)

We report the deposition of $\text{LiNb}_{1-x}\text{Ta}_x\text{O}_3$ ($0 \leq x \leq 1$) films on (001) sapphire substrates in soft vacuum using a radio frequency thermal plasma. The growth rate, crystallinity, c -axis orientation, and surface roughness were examined as functions of substrate temperature, precursor feed rate, and substrate surface condition. The film Nb/Ta ratio was well controlled by using an appropriate uniform mixture of lithium-niobium and lithium-tantalum alkoxide solutions. The epitaxy and crystallinity of the films were much improved when the film growth rate was raised from 20 to 180–380 nm/min, where the films with the (006) rocking curve full width at half maximum values as low as 0.12° – 0.2° could be produced. The film roughness could be reduced by using a liquid precursor with higher metal concentrations, achieving the root-mean-square value on the order of 5 nm. The refractive indices of the films are in good correspondence with their composition and crystallinity. © 2003 American Vacuum Society. [DOI: 10.1116/1.1582451]

I. INTRODUCTION

Thin films of ferroelectric oxide materials have been attracting great interest for numerous applications. Such applications include microactuators, optical waveguide devices, spatial sensors and detectors, surface acoustic wave devices, imaging devices, multilayer capacitors for memories, and piezoelectric film-based microelectromechanical systems.^{1,2}

Owing to their advantageous electro-optical, acousto-optical, piezoelectric, and nonlinear optical properties, lithium niobate (LiNbO_3 , LN) and lithium tantalate (LiTaO_3 , LT) are certainly among the most promising materials for integrated and guided-wave optics devices.^{1–4} Thus they are strongly desired as high quality thin films grown with good surface morphology on substrates with low refractive indices and high acoustic wave velocity. However, to date, applications of the unique physical properties of LN and LT, including large second-order optical nonlinearity, piezoelectric, pyroelectric, and elasto-optical effects, have been limited to devices fabricated from bulk crystals.^{2,4,5} Furthermore, lithium niobate-tantalate ($\text{LiNb}_{1-x}\text{Ta}_x\text{O}_3$, LNT) forms a continuous solid solution of LN and LT that is also a ferroelectric material. The physical properties of LNT vary with the Nb/Ta ratio from those of LN ($x=0$) to those of LT ($x=1$).^{6,7} This makes LNT, in many cases, an even more attractive material than LN or LT, because its physical properties can be tuned to meet engineering specifications.⁷

In recent years, a number of deposition techniques including liquid phase epitaxy (LPE),^{8–10} sputtering,^{11,12} molecular beam epitaxy (MBE),¹³ pulsed laser deposition (PLD),^{14–17} metalorganic chemical vapor deposition (MOCVD),^{5,18–20}

and sol-gel processing^{21–23} have been proposed to grow high-quality LN or LT layers mainly on sapphire substrates. The LN and LT films with the best quality have been reported to demonstrate optical losses less than 2 dB/cm, (006) rocking curve full width at half maximum (FWHM) values of 0.04° – 0.07° , and surface root-mean-square roughness (R_{rms}) values of 1.1–1.5 nm.^{5,12,20,22,23} However, there have been only a few reports on LNT film deposition. Kawaguchi *et al.* reported LNT film growth on LN substrates with $0 \leq x \leq 0.4$ using the LPE method.^{9,10} In their experiment, the film crystallinity considerably degraded when $x > 0.3$, due to the increase of lattice mismatch and growth temperature. More recently, Cheng *et al.* fabricated highly c -oriented LNT films with $x < 0.33$ on Si(111) substrates, using the sol-gel technique.⁶ They also found that the degree of c orientation was relatively low at $0.5 < x < 1$.

The thermal plasma spray CVD (TPS CVD) method using liquid source material was first applied by Yamaguchi *et al.*²⁴ for the preparation of preferentially oriented LN films with the deposition rate on the order of 100 nm/min, i.e., 10–100 times faster than those of the most conventional vapor deposition methods. It has been proposed that the main deposition species in the TPS CVD are clusters, by analogy with the thermal plasma flash evaporation process.^{24–26} More recently, we reported the deposition of LNT films (generally with $x \leq 0.5$) on both α - Al_2O_3 and silicon substrates and the control of their c -axis orientation.^{27–30} In order to meet technological requirements, it is important to develop films with large area and good crystalline quality. The crystallinity, texture, stoichiometry, and surface morphology of films are known to depend on the deposition temperature, growth rate, and other fabrication parameters. However, in the case of deposition from thermal plasma clusters, the possibilities of controlling film morphology, orientation, compositional ho-

^{a)} Author to whom correspondence should be addressed. Present address: Université du Québec à Chicoutimi, Chicoutimi, Québec, G7H 2B1, Canada electronic mail: kulinich@terra.mm.t.u-tokyo.ac.jp

mogeneity, and grain size are largely unknown. Therefore systematic studies are necessary to clarify whether or not thermal plasma processing can be applied for manufacturing high-quality ferroelectric films in the future.

In the present study, we apply the TPS CVD technique to grow $\text{LiNb}_{1-x}\text{Ta}_x\text{O}_3$ films on (001)-oriented sapphire within the entire Ta ($0 \leq x \leq 1$) composition. The influence of the key deposition parameters, i.e., temperature, growth rate, substrate surface, and starting material concentration on fabricated films' characteristics is investigated systematically. The optical properties (refractive index) of the films are estimated and related to their Ta content and crystallinity.

II. EXPERIMENTAL PART

A. Film deposition

Details of the experimental procedure and scheme of the plasma chamber have been given elsewhere.^{24,27,28} Lithium-niobium and lithium-tantalum alkoxide metalorganic solutions for dip coating [$\text{LiNb}(\text{OR})_6$ and $\text{LiTa}(\text{OR})_6$ in 3-methylbutyl acetate as a solvent from Kojundo Co., Japan] were used as liquid precursors. The concentration of metals in each individual precursor solution corresponded to 3 wt % LiNbO_3 or LiTaO_3 , respectively. These solutions were mixed in the various molar ratios in order to obtain suitable proper source materials. For comparison, a similar lithium-niobium alkoxide solution with a higher metal concentration (10 wt % of LiNbO_3) was sprayed in several experiments to examine the effect of the subproduct H_2O and CO_2 during deposition. As-supplied mechanochemically polished, as well as annealed at 1000 or 1400 °C, (001)-axis sapphire substrates from Earth Chemical Co. Ltd., Japan were cleaned with acetone and ethanol prior to use.

Compared with the work of Yamaguchi *et al.*,²⁴ we used a modified TPS CVD chamber, in which the plasma blowing direction was vertically upward.^{27–29} A liquid solution containing metalorganic precursors was fed into a radio frequency O_2 -Ar thermal plasma as a mist from the injection probe. The substrate temperature (T_{sub}) was normally controlled within the accuracy of ± 5 –20 °C, depending on the liquid feed rate R , and was directly monitored by measuring the infrared radiation from the reverse side of the substrate, covered with golden foil, through an optical fiber. Table I gives a summary of the experimental conditions.

B. Film characterization

The films were studied in a Hitachi S-4200 field emission scanning electron microscope (SEM), and the thickness was measured on fractured cross-section samples. The film growth rates, estimated from the film thickness, were deduced to depend linearly on the liquid feed rate R applied. They were within the range of 20–500 nm/min, when R was changed from 0.5 to 10 ml/min for the low-concentration precursor (3 wt % of LNT), and within the range of 90–500 nm/min, when the high-concentration precursor (10 wt % of LN) was applied at $R = 0.6$ –4.0 ml/min.

TABLE I. Summary of experimental conditions.

Source Ta/(Nb+Ta) ratio, x	0–1.0
Power (kW)	46
Pressure (Torr)	150
O_2 tangential gas flow rate (l/min)	45
Ar carrier gas flow rate (l/min)	3
Ar spray gas flow rate (l/min)	3.6
Ar inner gas flow rate (l/min)	5
Liquid feed rate, R (ml/min)	0.5–10
Deposition temperature, T_{sub} (°C)	570–800
Torch-substrate distance (cm)	37
Deposition time (s)	0.5–540
Substrate	(001) α - Al_2O_3
Typical LNT film thickness (nm)	170–200

The microstructure of the as-deposited samples was studied using a Hitachi 9000 NAR transmission electron microscope (TEM), being operated at 300 kV. The cross-sectional sample preparation procedure for TEM has been described elsewhere.³⁰ Phase identification and film orientation were provided using the conventional θ - 2θ scan x-ray diffraction (XRD) method and TEM. The (001) out-of-plane alignment (crystallinity) of the films was determined by XRD rocking curve analysis (θ scan).

The film composition was determined by inductively coupled plasma atomic emission spectroscopy (ICP AES) after the films had been completely dissolved in a hot HF - H_2SO_4 mixture on a sand bath. The instrumental uncertainties in determining the metal concentrations were less than $\pm 3\%$ and $\pm 5\%$ for Ta (Nb) and Li, respectively.

The surface morphology was examined by SEM and atomic force microscopy (AFM) using a Digital Instruments NanoScope IIIa, being operated in tapping mode with a Si tip. The R_{rms} values, calculated by geometric average, were determined for the observed area size of $2 \times 2 \mu\text{m}^2$. In addition, high-resolution field emission SEM (HRSEM), Hitachi S-5000, was applied to examine the initial growth behavior of LNT on the substrate surface. The refractive index was evaluated by means of spectroscopic ellipsometry.

III. RESULTS

A. Film composition and lattice parameters

$\text{LiNb}_{1-x}\text{Ta}_x\text{O}_3$ ($0 \leq x \leq 1$) films were deposited using seven precursor solution mixtures with the Nb:Ta ratios ranging from 1:0 to 0:1. Figures 1(a) and 1(b) show the change of the hexagonal c lattice parameter, calculated based on the (006) plane, and the $x = \text{Ta}/(\text{Nb} + \text{Ta})$ ratio in deposited LNT films as functions of the $x = \text{Ta}/(\text{Nb} + \text{Ta})$ ratio in the liquid source material. Figure 1(a) reveals that the c -axis lattice parameters of LNT films were somewhat lower than those of the bulk materials. They decrease from 13.84 to 13.72 Å with increasing the tantalum content, $x = \text{Ta}/(\text{Nb} + \text{Ta})$, from 0 to 1.0, while the bulk LNT specimens with $x = 0, 0.5$, and 1.0 exhibit c parameters equal to 13.862, 13.815, and 13.755 Å, respectively, as also shown in Fig. 1(a). The a -axis lattice parameters were calculated based on the (104) and (110) planes to be correspondingly somewhat higher than those in bulk materials of similar stoichiometry. These results imply

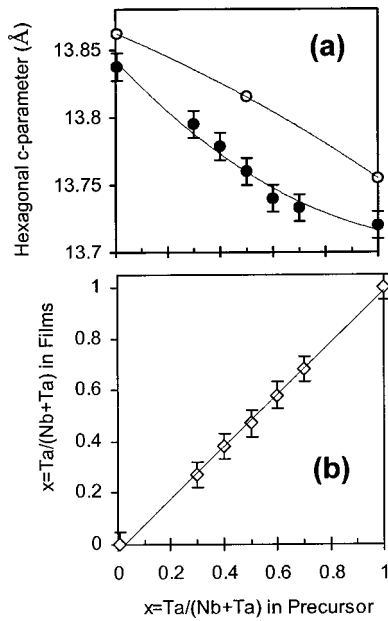


FIG. 1. Variations of $\text{LiNb}_{1-x}\text{Ta}_x\text{O}_3$ film hexagonal cell c parameter (a) and the $x = \text{Ta}/(\text{Nb} + \text{Ta})$ ratio in deposited films (b) with the $x = \text{Ta}/(\text{Nb} + \text{Ta})$ ratio in liquid source material (closed circles and open diamonds, respectively); film thickness was 170–200 nm for (a) and 150–600 nm for (b); for comparison, three points for bulk materials are also shown with open circles. Solid lines are given only as visual guides.

the existence of planar tensile stress of the (001)LNT film plane and film compression along the c axis. Figure 1(b), which is almost the same as reported previously,²⁹ presents the change of the film chemical composition with an initial solution composition, as measured by the ICP AES method. It is seen that the Ta content in the deposited films linearly increases with increasing initial Ta content in the liquid source material and is very close to the latter, thus indicating a precise control of the film composition by the deposition method. This is also in good agreement with the Nb/Ta ratios of the TPS CVD-fabricated films on Si substrates, measured by energy-dispersive x-ray spectroscopy,^{28,31} where good composition control was demonstrated as well. The metal ratio, $\text{Li}/(\text{Nb} + \text{Ta})$, in deposited LNT films was estimated to be from 1.0 to 1.1.

As discussed below and similar to TPS CVD-grown LNT films on Si substrates,^{28,31} in addition to those of the dominant $\text{LiNb}_{1-x}\text{Ta}_x\text{O}_3$ phase, weak additional (222) and (444) peaks of the Li-rich phase (LR), $\text{Li}_3(\text{Nb},\text{Ta})\text{O}_4$, as well as a set of very weak peaks of the Li-deficient phase (LD), $\text{Li}(\text{Nb},\text{Ta})_3\text{O}_8$, were also observed by XRD in LNT films deposited at $T_{\text{sub}} \leq 630\text{--}650^\circ\text{C}$ on sapphire.

B. Orientation and crystallinity

Since the electro-optical properties of LNT material are anisotropic and are strongly influenced by structural defects, growing epitaxial films and controlling their orientation and crystallinity are very important issues. Since both LNT and sapphire have hexagonal crystal structures and the latter has a lower refractive index, sapphire is a good candidate for

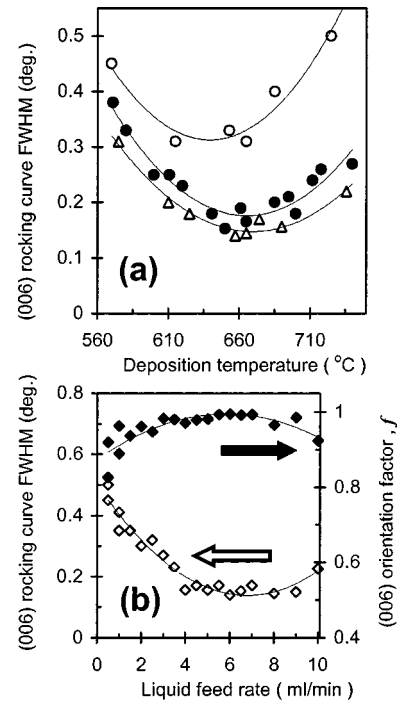


FIG. 2. (a) Variation of $\text{LiNb}_{0.5}\text{Ta}_{0.5}\text{O}_3$ (006) rocking curve FWHM as a function of deposition temperature T_{sub} ; all of the films have a similar thickness of approximately 170–200 nm; three dependencies for $R = 1$ ml/min (open circles), $R = 4$ ml/min (closed circles), and $R = 8$ ml/min (triangles) are shown for comparison. (b) Variation of $\text{LiNb}_{0.5}\text{Ta}_{0.5}\text{O}_3$ (006) rocking curve FWHM (open diamonds) as a function of liquid precursor input at $T_{\text{sub}} = 650\text{--}670^\circ\text{C}$; the change of the (006) orientation factor for the same samples (closed diamonds) is also given. The solid lines are given only as visual guides.

growing heteroepitaxial LNT films for a variety of optical and electro-optical applications. However, a rather large lattice mismatch on the order of 8%¹⁶ makes the deposition of smooth epitaxial LNT films with high crystalline quality on (001) $\alpha\text{-Al}_2\text{O}_3$ difficult.^{5,12,16,19,23}

X-ray patterns of highly c -axis oriented TPS CVD-fabricated LNT films have been reported earlier.^{29,30} The c -axis orientation degree (or orientation factor) f , which was previously applied for describing the degree of (006)-orientation of LN and LNT films,^{6,15,28,29} is used in this work to evaluate a film (006)-texture, too. [The parameter is defined as $f = [I_r(006) - I_r^{\text{powder}}(006)] / [1 - I_r^{\text{powder}}(006)]$, where relative intensity $I_r(006)$ is the XRD intensity of the (006) peak normalized by the sum intensity of all the peaks of LNT between $2\theta = 20^\circ$ and 60° and $I_r^{\text{powder}}(006)$ is the same value for LNT powder. For randomly oriented polycrystalline films or powders, $f = 0$; for completely (006)-oriented LNT films, $f = 1$; and for partially oriented films, $0 < f < 1$.] It should be mentioned that at optimal conditions, the 170–200-nm-thick LNT films in this study reached the c -axis orientation degree value as high as $f = 0.98\text{--}1.00$.

Figure 2(a) shows the film (006) rocking curve FWHM values as a function of substrate temperature T_{sub} for the three growth rates of 40–50 (open circles), 180–190 (closed circles), and 360–380 nm/min (triangles). Since the results of rocking-curve XRD measurement are affected by film

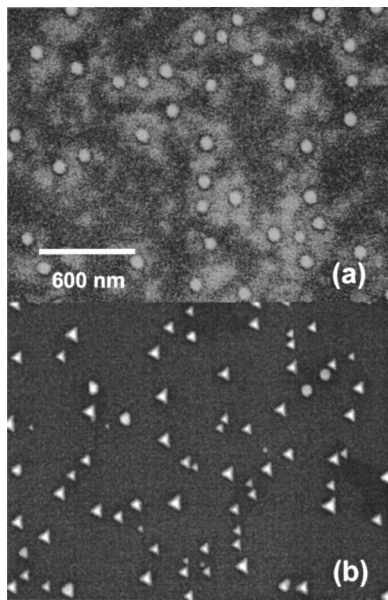


FIG. 3. HRSEM images of two LNT samples deposited onto as-supplied (001) sapphire for 0.5 s at $T_{\text{sub}}=650^\circ\text{C}$ and liquid feed rate $R=2$ ml/min (a) and $R=8$ ml/min (b); nominal growth rates correspond to 90–100 and 360–380 nm/min, respectively.

thickness, all of these films have similar thicknesses of 170–200 nm. Rocking curve widths are seen first to decrease with increasing T_{sub} , implying the improvement of crystalline quality. Then, after they exhibit a small temperature dependence (at 640–710 $^\circ\text{C}$ for 180–190 and 360–380 nm/min and at 610–660 $^\circ\text{C}$ for 40–50 nm/min), broadening of the (006) rocking curve FWHM starts again at elevated T_{sub} , indicating LNT film crystallinity deterioration. The latter effect, as has been reported previously,³⁰ is accomplished by the change from the (006) texture to the (012) orientation of LNT films, as well as to (104) and/or (110) texturing in many cases. Figure 2(b) presents the variation of the film crystallinity and (006)-orientation degree as functions of liquid feed rate (corresponding to growth rates of approximately 20–500 nm/min) at the fixed deposition temperature kept at 650–670 $^\circ\text{C}$. It is seen that at a constant average T_{sub} , both the c -axis orientation degree and crystallinity of LNT films are much improved by employing an increased source input until $R\leq 8$ to 9 ml/min (growth rates up to 380–440 nm/min).

TEM observation revealed that a large part of LNT films grew epitaxially.^{30,32} Moreover, the epitaxial relation was significantly improved when the liquid feed rate R was raised from 0.5–1.0 (where a thin amorphous interlayer between films and substrates was often observed^{30,32}) to 7.0 ml/min;³² and this is in good agreement with Fig. 2. Figure 3 presents HRSEM surface images for two LNT samples deposited onto the as-received sapphire at $R=2$ (a) and 8 ml/min (b) for a short period of 0.5 s. Before the HRSEM examination, the samples were sputter-coated with approximately 2-nm-thick Pt, and therefore some difference in contrast might result from the relatively nonuniform Pt coatings of the two specimens and/or from different instrumental adjustment during

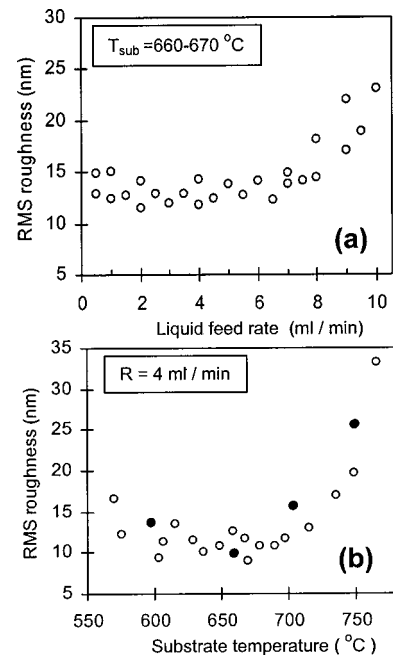


FIG. 4. Change of R_{rms} roughness as a function of (a) liquid feed rate R employed and (b) average substrate temperature during deposition. The films examined are of similar composition $\text{LiNb}_{0.5}\text{Ta}_{0.5}\text{O}_3$ and thickness of around 170–200 nm. AFM images for the films marked in black are shown in Fig. 5.

observations. It is seen that at a same deposition temperature the LNT nucleation behavior differs when liquid precursor's feed rate (and consequently, film growth rate) is changed.

In contrast to the results of Kawaguchi *et al.*^{9,10} and Cheng *et al.*,⁶ under optimal substrate temperatures and growth rates, the (006) rocking curve FWHM values of the LNT films were almost constant and were independent of the tantalum composition within the entire Ta content range $0\leq x\leq 1$. The narrowest rocking curve width obtained for 170–200-nm-thick LNT films in this study was observed to be 0.12° . Also, in contrast to the report of Feigelson,¹⁹ the LNT 170–200-nm-thick films did not exhibit any cracking, although thicker films of 400–600 nm have often been found to demonstrate cracking on cooling.

C. Surface morphology

Optical and electrical properties of LNT films are strongly influenced by their surface morphology and structural defects. Previous work has shown that surface scattering can account for up to 50% of the optical loss in a thin film.²

Figures 4(a) and 4(b) present two independent series of experiments which show the influence of the liquid feed rate R (corresponding to growth rates from 20 to 500 nm/min) at constant $T_{\text{sub}}=660$ –670 $^\circ\text{C}$ and the substrate temperature T_{sub} at a growth rate of 180–190 nm/min on the average surface roughness of LNT films. It is seen that films exhibit small feed-rate and T_{sub} dependences of their R_{rms} at $R<8$ ml/min and $T_{\text{sub}}<700^\circ\text{C}$, respectively, and the roughness value $R_{\text{rms}}=9.5$ –14 nm can be achieved at these condi-

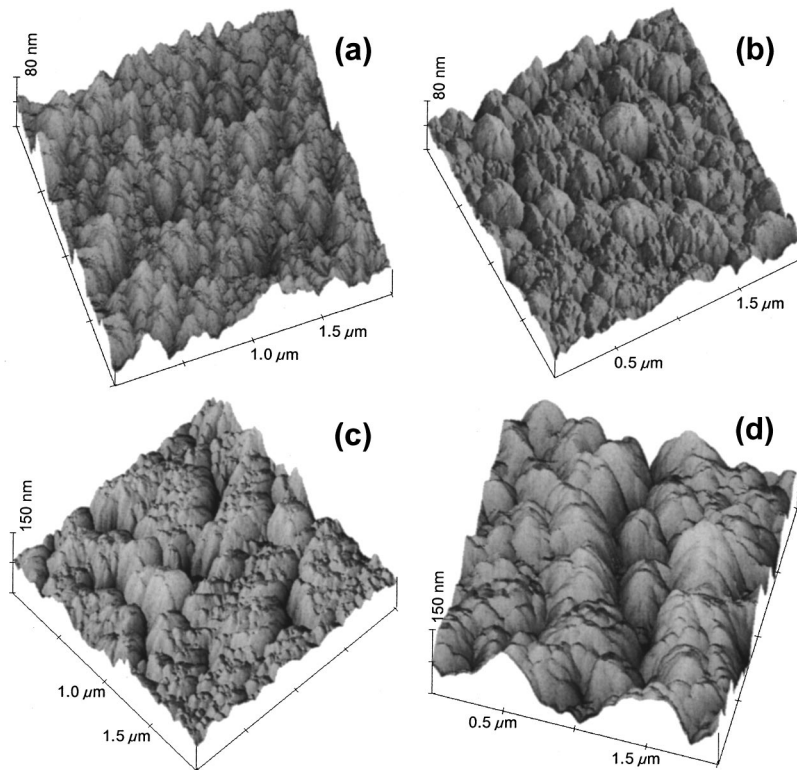


FIG. 5. Change of $\text{LiNb}_{1-x}\text{Ta}_x\text{O}_3$ ($x=0.5$) film surface morphology as a function of average deposition temperature: (a) 595°C ($R_{\text{rms}}=14.2$ nm), (b) 660°C ($R_{\text{rms}}=10.1$ nm), (c) 703°C ($R_{\text{rms}}=15.6$ nm), and (d) 750°C ($R_{\text{rms}}=25.8$ nm); $2 \times 2 \mu\text{m}^2$ areas are shown. The films were grown to 170–200 nm thickness at 180–190 nm/min.

tions. In addition, Fig. 5 gives AFM surface images for several films fabricated at different temperatures which are marked in Fig. 4(b) with closed circles.

To examine the effect of plasma composition on the films' roughness, in some experiments, a LN liquid precursor with 10 wt% of LN was used. Since this precursor provides roughly 3.33 times less organic material at the same film growth rate (and consequently, lower H_2O and CO_2 concentrations) for the plasma, this was expected to have a significant effect on the entire deposition process. In fact, several LN films fabricated with such a precursor demonstrated R_{rms} values of 5–10 nm, whereas the LNT films grown at the same $T_{\text{sub}}=650\text{--}700^\circ\text{C}$ and growth rates of 180–500 nm/min normally had $R_{\text{rms}} \geq 10$ nm (Fig. 4). Figure 6 presents an AFM surface image of the LN 190-nm-thick film deposited using a 10 wt% LN metalorganic precursor at 190 nm/min and T_{sub} at approximately 680°C . The film demonstrates reduced surface R_{rms} of 4.9 nm.

D. Influence of substrate surface

It is well known that as-supplied sapphire substrates are produced with mechanochemical mirror polishing and therefore their topmost surface has irregular corrugations and crystallographic defects.³³ Thus the atomic-scale flatness of the substrate surface obtained by high-temperature annealing of commercial sapphire^{5,19,33,34} is expected to enhance the epitaxial growth of LNT ($0 \leq x \leq 1$) films.^{33,34}

Figure 7 presents x-ray patterns for the LNT ($x=0.5$) films deposited onto annealed (001) sapphire substrates. The substrates, whose surface topographies are presented in Fig. 8, were heat treated at 1400°C for 2 h [Figs. 7(b) and 7(c)]

and 1000°C for 1 h [Fig. 7(a)]. The deposition temperature employed was $T_{\text{sub}}=640\text{--}650^\circ\text{C}$, which normally resulted in LNT films with very high (006) orientation on as-supplied substrates (f on the order of 0.95–1.0). It is seen that on substrates annealed at 1400°C [Figs. 7(b) and 7(c)] the films had significantly lower (006)-texture and crystallinity, which were improved by using the substrate after a softer annealing [Fig. 7(a)].

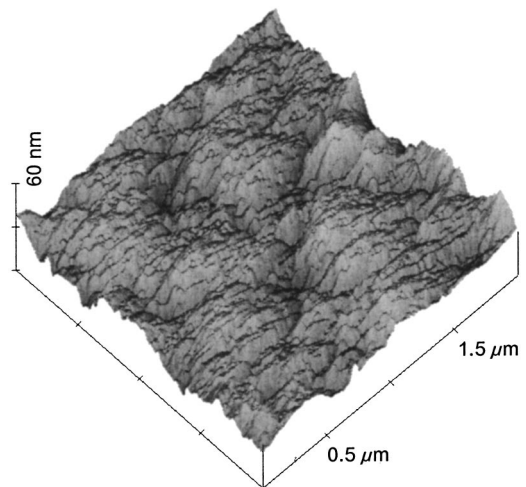


FIG. 6. AFM surface morphology image of LiNbO_3 190 nm thick film on as-supplied substrate grown from highly concentrated (10 wt% LN) precursor at $680 \pm 3^\circ\text{C}$ and 190 nm/min. The average roughness estimated for the $2 \times 2 \mu\text{m}^2$ area is $R_{\text{rms}}=4.9$ nm.

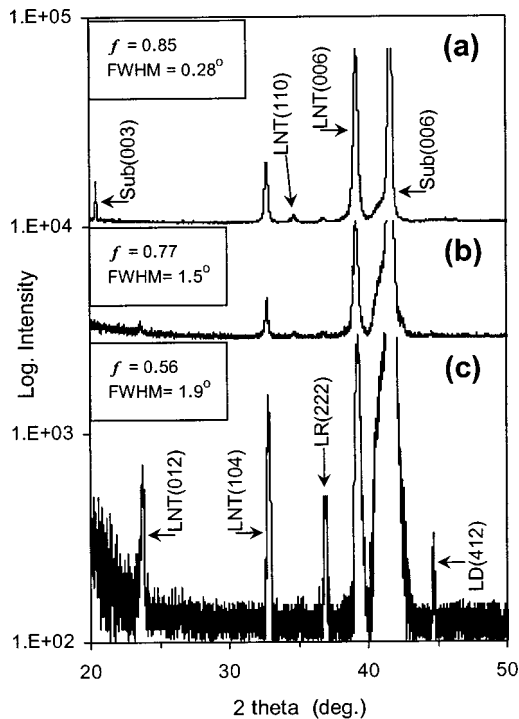


FIG. 7. X-ray patterns (logarithmic intensity) of LNT films grown on annealed (001) sapphire at $T_{\text{sub}} = 640\text{--}650\text{ }^{\circ}\text{C}$. Annealing temperature and deposition rate were: $1000\text{ }^{\circ}\text{C}$ (1 h) and 360 nm/min (a); $1400\text{ }^{\circ}\text{C}$ (2 h) and 360 nm/min (b); and $1400\text{ }^{\circ}\text{C}$ (2 h) and 180 nm/min (c), respectively. Films were grown to be approximately $170\text{--}200\text{ nm}$ thick, and their (006) orientation factors and crystallinities are indicated.

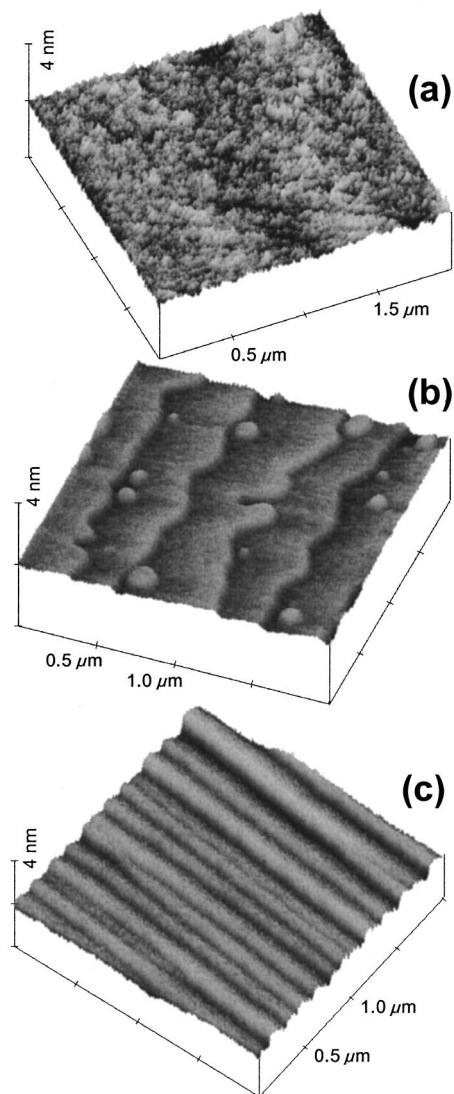


FIG. 8. Surface morphology of (001) sapphire used: (a) as-supplied, (b) heat treated at $1000\text{ }^{\circ}\text{C}$ for 1 h, and (c) heat treated at $1400\text{ }^{\circ}\text{C}$ for 2 h; $2 \times 2\text{ }\mu\text{m}^2$ areas are shown.

E. Refractive index

In order to estimate the optical quality of the LNT films, the ellipsometric spectra were analyzed by multilayer modeling of the three-layer (air, film, and substrate) system. The unknown optical constants of the LNT films were determined by fitting the model function to the measured data,³⁵ and a least-squares-fitting procedure was used to obtain the fitting parameters and thicknesses of the LNT films. The estimated film thicknesses were in good agreement with the values measured by SEM. The ellipsometric method does not allow the separation of the two indices of anisotropic LNT material (ordinary n_o and extraordinary n_e , which are in the direction normal to the c axis and along the c axis, respectively). Therefore, only one index, n , was obtained. Figure 9 shows the refractive index dependence on wavelength, as evaluated from the ellipsometric measurements of the $170\text{--}200\text{-nm}$ -thick $\text{LiNb}_{1-x}\text{Ta}_x\text{O}_3$ films fabricated with (a) different chemical composition ($x = 0.5, 0.6, \text{ and } 0.7$) and (b) different crystallinity [(006) rocking curve FWHM values of 0.19° , 0.35° , and 0.47°].

IV. DISCUSSION

A. Film composition and lattice parameters

The observed film planar tensile stress of the (001) LNT plane is caused by the difference in the thermal expansion coefficients of the film and substrate. As reported in our pre-

vious work,³⁰ the film lattice parameters remained unchanged after annealing in air at $750\text{ }^{\circ}\text{C}$ for 6 h, which may be additional evidence that the LNT films are under tensile stress. This agrees well with the data of Veignant *et al.*,¹⁶ who reported the mismatch parameter between the LN film and (001) $\alpha\text{-Al}_2\text{O}_3$ substrate to be 8.6% at $750\text{ }^{\circ}\text{C}$.

Figure 10 presents further evidence of the existence of film compressive stress along the $\langle 006 \rangle$ direction. It is seen that the crystal lattice of the films becomes more relaxed when their thickness is increased. However, even for the $1.15\text{ }\mu\text{m}$ thick film, the hexagonal c parameter still seems to be far from a constant value. It is worth noting here that even LPE-formed LN films on LN substrates have been reported by Kawaguchi *et al.*⁸ to reach a constant c lattice parameter at approximately $>15\text{--}20\text{ }\mu\text{m}$ thickness. It is also seen from Fig. 10 that the degree of (006)-orientation gradually degraded with film thickness, and thus a decrease of film quality could be expected. In fact, even though at $1.15\text{ }\mu\text{m}$ the

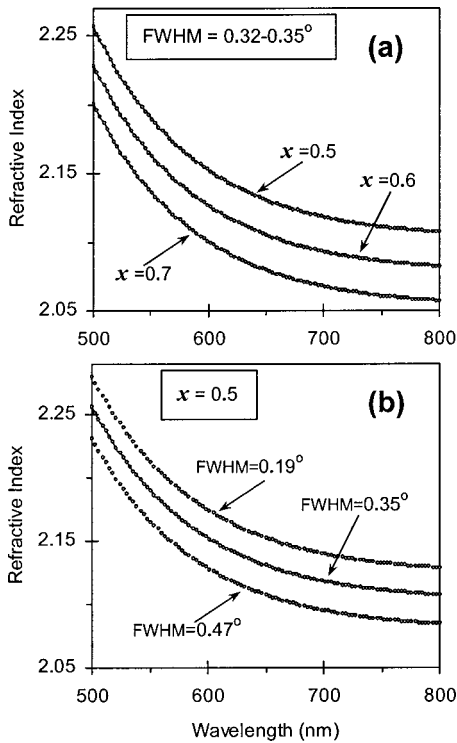


FIG. 9. Refractive index n for $\text{LiNb}_{1-x}\text{Ta}_x\text{O}_3$ 170–200-nm-thick films, deposited onto as-received (001) sapphire substrates, as measured by spectroscopic ellipsometry. (a) Variation with film composition ($x=0.5, 0.6,$ and 0.7); all of the films were obtained at 90 nm/min and $T_{\text{sub}}=675 \pm 10^\circ\text{C}$; their (006) rocking curve FWHM was $0.32^\circ\text{--}0.35^\circ$. (b) Variation with film crystallinity; all of the films have the same composition, $x=0.5$.

film still has quite a strong c -axis orientation ($f=0.89$), it is optically opaque, which is probably caused by both increased surface roughness and decreased crystallinity.

The measured value of the metal ratio $\text{Li}/(\text{Nb}+\text{Ta})$, which was between 1.0 and 1.1, may be attributed to the somewhat low sensitivity of the ICP AES technique to Li content at low concentrations and, consequently, the lower accuracy of measurement of its concentrations. This suggestion is confirmed by the finding that all thicker LNT films

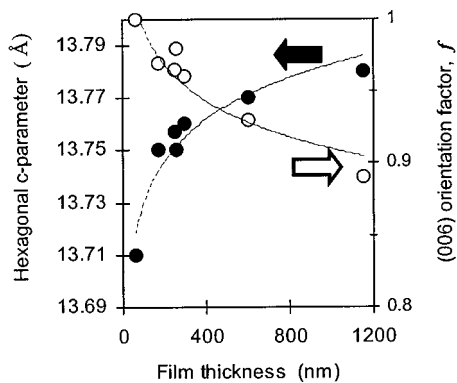


FIG. 10. Variation of $\text{LiNb}_{0.5}\text{Ta}_{0.5}\text{O}_3$ film hexagonal cell c parameter and degree of orientation with thickness. The films were deposited onto as-received (001) sapphire substrates at 180 nm/min and $T_{\text{sub}}=670 \pm 10^\circ\text{C}$ for 5 s to 9 min. Solid lines are only visual guides.

analyzed were found to have $\text{Li}/(\text{Nb}+\text{Ta})$ ratios very close to 1.0, whereas the value 1.1 was typical for thinner films, which after dissolution gave Li concentrations comparable with the lowest determination limit for this element. Thus, within the accuracy of our analysis, LNT films were considered to be nearly stoichiometric.

A slight inhomogeneity of the films fabricated at relatively lower deposition temperatures [see Fig. 7(c)] is believed to result from the fast deposition from clusters, which can have a compositional distribution, thus yielding some film areas with slightly different metal (Li, Nb, Ta) concentrations. When LNT films are fabricated at high rates (on the order of several tens or hundreds nm/min) from such clusters at relatively low temperatures, in this case the surface species mobility and film bulk diffusion are limited. As a result, some compositional deviation of the film areas may be expected. This is in good agreement with the fact that the peaks of Li-rich (LR) and Li-deficient (LD) phases became weaker and finally disappeared when elevated growth temperatures were applied. The fact that the above additional peaks decreased/disappeared after postdeposition air annealing of LNT films is further evidence of this assumption.

B. Orientation and crystallinity

The behavior of LNT film crystallinity as determined by XRD measurements at different substrate temperatures, shown in Fig. 2(a), is not well understood thus far. A similar trend has been observed by Lee and Feigelson on both sapphire and Si substrates,^{5,20} although their MOCVD method provided considerably lower film growth rates on the order of 1–5 nm/min. They have explained the degradation of LN film crystallinity on sapphire as a result of the vapor phase nucleation of LN metalorganic precursor particles at higher T_{sub} .⁵ At the same time, for Si substrate the surface free-energy anisotropy approach has been proposed.²⁰ The latter suggests that at higher temperatures, ad-species can attain sufficient surface mobility to rearrange themselves into grains with the lowest surface free energy, which is assumed to be the (012) plane for LNT materials,^{5,14} parallel to the substrate surface.^{20,36} This change from the (006) to the (012) texture leads, in turn, to deterioration of film crystallinity. Since, in contrast to the MOCVD employed by Lee and Feigelson,⁵ in our experiment the deposition species are expected to be thermal clusters,^{25,26} it is reasonable to assume that it is enhanced surface mobility that is responsible for the FWHM line broadening at elevated T_{sub} in Fig. 2(a), rather than any gas phase nucleation of metalorganic molecules.

The tendency of a growing surface to lower its surface free energy through film orientation at a sufficiently high surface mobility of deposited particles is well known.^{20,36} On this basis the shift of LNT film FWHM broadening at higher growth rates towards higher deposition temperatures can be explained. Actually, since the key factor, surface mobility, governing the change in film orientation is suppressed by higher material flux, the (006) texture of growing LNT films

can be maintained at elevated T_{sub} , as seen in Fig. 2(a) and confirmed in Fig. 2(b).

To explain the reason for some decrease of film crystallinity and (006) texture in Fig. 2(b) at $R=9$ to 10 ml/min, we assume that larger clusters formed at high initial source input R might be then imbedded into the growing film, thus giving rise to some deterioration of both film orientation and crystallinity. However, we also cannot exclude the effect of higher H_2O and CO_2 gas concentrations in plasma, which become quite considerable when a larger amount of precursor ($R=9$ to 10 ml/min) is injected.

It is interesting that the behavior of crystallinity and orientation of TPS CVD-grown films demonstrates many similarities, with respect to T_{sub} and growth rate parameters, to that of MOCVD-deposited LN films on Si substrate, where no epitaxial relation is expected and high film textures are governed by growth rate anisotropy or surface free-energy anisotropy effects at low and high surface mobilities, respectively.²⁰ Even though many aspects of such similarities are still not clear, we suppose that they result from the fast deposition process with clusters on the order of a few nm as the main acting species.

It should also be added that, in addition to the (012)-oriented LNT grains which are assumed to have the lowest surface free energy,^{14,20} in our experiments (104)- and (110)-textured grains were also generally deposited at elevated substrate temperatures. Note that this observation agrees well with that of Wu *et al.*,¹⁴ who have also reported the occurrence of the three additional orientations for PLD-formed LN films on fused silica at $T_{\text{sub}} \geq 650^\circ\text{C}$. Thus, taking into consideration the above-mentioned surface free-energy anisotropy effect, we suggest that it is likely that the surface free energies for the two LNT surfaces, i.e., (104) and (110) planes, might be also lower than that of the (006) surface. Therefore, under the conditions of a high T_{sub} and fast deposition, LNT grains with (104) and (110) orientation can also nucleate and grow.

Even though the details of the nucleation mechanism are not yet clear and some additional parameters (e.g., plasma gas contents, see below) still require further systematic examination, it is seen in Fig. 3 that when the growth rate was increased from 90–180 to 360–380 nm/min, the shape of the LNT particles formed markedly changed from a dome-like shape to a well-oriented triangular-pyramidal one. Furthermore, the number of deposited islands seems to be larger, and their surface distribution is also more uniform in Fig. 3(b). The cross-sectional TEM observations of the round and triangular islands in Figs. 3(a) and 3(b) revealed their mainly amorphous nature and the dome-like shape (a) and the well-crystallized, highly epitaxial and triangular-pyramidal shape (b), respectively. Taking into account all of the above data, it is thus seen that LNT films on sapphire deposited at higher growth rates have better crystallinity and epitaxial relation even from the very initial growth stage.

It is well known that LN or LT film growth from a vapor phase on sapphire follows a three-dimensional (Volmer–Weber or Stranski–Krastanov) or island mode.^{5,16,30,33} From

this point of view, more uniform LNT initial island distribution on the surface seems to be more advantageous, as giving a more uniform island coalescence and lower surface roughness.⁵ The LNT clusters formed in the plasma boundary layer under higher raw material input [as in the case of $R=8$ ml/min, Fig. 3(b)] are thought to have a greater average size and accumulation of internal energy than those formed at a lower material input [$R=2$ ml/min, Fig. 3(a)], which further provides them with a higher rearrangement/crystallization ability on the surface. However, one must also keep in mind that the cluster formation gas media (the contents of O_2 , H_2O , and CO_2 gases and their various ions, which differ with different metalorganic material input) might also influence both the initial and further growth behaviors of LNT films, and this influence has not been studied in detail thus far.

As previously reported, TPS CVD-grown LNT films in general have some amount of twins.²⁹ Their number, however, is seriously reduced at optimal growth rates of 180–380 nm/min,³² which probably can be attributed to higher energy of clusters as deposited species at these conditions. The twinned grains, which can be described as a 60° rotation of the LNT structure about the c axis and have only different in-plane relation to the substrate, are energetically less favorable^{5,16} and tend to disappear at higher deposition temperatures or during postdeposition annealing.^{5,16,19} We also detected LNT films which were free of twinned grains when T_{sub} applied was larger than 710°C .²⁷ This is in good agreement with the results of a number of investigators who used different deposition methods to produce epitaxial LN films on sapphire.^{5,16,17,19,22} Interestingly, however, Lansiaux *et al.*¹² were able to fabricate magnetron-sputtered LN films on (001) sapphire with almost no 60° rotated grains even at such a low T_{sub} as 490°C .

C. Surface morphology

The reason for the film surface deterioration at $R > 8$ ml/min in Fig. 4(a) is not well understood so far. Such behavior can be attributed to a number of factors. On the one hand, somewhat less reliable temperature control at higher liquid feed rates (caused by a greater amount of oxidation reaction heat from plasma) results in more frequent deviations of T_{sub} ; on the other hand, a larger amount of metalorganic materials injected at higher raw material input might change the gas media over the growing film (giving more gaseous H_2O and CO_2), which could also influence the surface morphology. Again, as in the case of crystallinity deteriorated at increased feed rates, the possible formation/incorporation of larger clusters/particles could also increase R_{rms} .

It is seen in Fig. 5(a) that at relatively lower substrate temperatures ($T_{\text{sub}} < 600^\circ\text{C}$), where LNT film crystallinity is believed to be poorer due to the limited surface mobility, films with a greater aspect ratio of grain height to diameter are formed. When T_{sub} is then raised to 660°C , owing to the enhancement of both surface diffusion and lateral grain growth, the grains coalesce with a lower aspect ratio and

much better crystallinity [Fig. 2(a)]. As a result, surface roughness decreases in the temperature range $T_{\text{sub}} = 600\text{--}690\text{ }^{\circ}\text{C}$, where the films with $R_{\text{rms}} = 9.5\text{--}12.5\text{ nm}$ are grown [Figs. 4(b) and 5(b)]. At $T_{\text{sub}} \geq 700\text{ }^{\circ}\text{C}$, as a result of the further increase of grain size, larger valleys between them are formed and developed. Consequently, the surface roughness starts increasing again [Fig. 4(b)], which is well observed in Figs. 5(c) and 5(d) where gradual surface grooving at elevated temperatures is shown.

The above observations on significant surface roughening at elevated T_{sub} are consistent with those reported by Lee and Feigelson,⁵ who also fabricated their LN films from vapor phase. Moreover, the surfaces of sol-gel-fabricated LN films were reported by Ono *et al.*²¹ to degrade from being quite smooth at heat-treatment temperatures below $500\text{ }^{\circ}\text{C}$ to being quite rough at $700\text{ }^{\circ}\text{C}$. Therefore surface roughening may be considered as a general tendency of LNT films at increased fabrication temperatures and appears to result from the lattice mismatch between the LNT film and the sapphire substrate.

The LN film in Fig. 6, deposited from a highly concentrated precursor, demonstrates a lower $R_{\text{rms}} = 4.9\text{ nm}$. This means that using highly concentrated precursors may be quite promising with respect to improvement of the LNT film surface smoothness in the future. The important point, however, to be overcome is the rapid increase of viscosity of metalorganic solutions, when their concentration of metal alkoxides is raised. On the other hand, the film's somewhat lower crystallinity (rocking curve FWHM = 0.47°) and (006) texture ($f = 0.9$) imply that for the new precursor the deposition parameters have to be further optimized.

D. Influence of substrate surface

As a result of a high-temperature predeposition substrate heat treatment, the number of active sites (and consequently, the number of LNT nuclei formed) on the substrate is thought to decrease markedly, allowing grains with (012) and (104) orientation to be formed, as shown in Fig. 7(c) and discussed previously. However, the (006) LNT film orientation was somewhat improved from $f = 0.56$ to 0.77 when the growth rate used was increased [Fig. 7(b)]. This observation is also in good agreement with the above discussion, implying that this occurred as a result of suppressing the surface ad-species mobility which in turn led to a better c -axis orientation (see Secs. III B and IV B). Then, when the substrate with less regular terraces was used, the film (006) orientation was further improved, as shown in Fig. 7(a). Note that peak intensities are plotted along a logarithmic scale in Fig. 7, thus implying a constant (006) peak intensity increase from sample (c) to (b) to (a).

It is seen in Fig. 8(a) that the as-received (001) $\alpha\text{-Al}_2\text{O}_3$ has irregular small scratches and crystallographic defects, resulting from mechanochemical polishing, as revealed in part by Shtansky *et al.* with cross-sectional TEM.³⁰ The surface of the substrate after 1 h heat treatment at $1000\text{ }^{\circ}\text{C}$ [Fig. 8(b)] demonstrates obvious surface restructuring and a set of atomically flat terraces with the step height around 0.22 nm

($c/6$), which started forming and will become straight with higher annealing temperatures or longer annealing time. In contrast, Fig. 8(c) shows variable step heights of $c/6$, $c/3$, and $c/2$ adjacent to one another and with straight atomically flat terraces, which is in good agreement with previous works.^{5,19,33,34} It is believed that the surface in Fig. 8(c) has fewer defects than that in Fig. 8(b) and thus provides a lower LNT film nucleation density, as discussed above.

It should be added that detailed comparison of the present results on annealed (001) sapphire and those from the previous works^{5,19,33,34} confirm that the final sapphire surface depends significantly on annealing temperature and duration. Taking into account the data of Fig. 7 and those presented in the above sections, very thorough optimization of both the heat-treatment process and the TPS CVD conditions is needed to improve LNT films on atomically flat sapphire.

E. Refractive index

As seen in Fig. 9(a) and expected for LNT materials,⁷ the index of refraction for the films produced at the same growth rate of $90\text{--}100\text{ nm/min}$ and growth temperature $T_{\text{sub}} = 675 \pm 10\text{ }^{\circ}\text{C}$ (and therefore, having similar crystallinity) decreases with the Ta content $x = \text{Ta}/(\text{Nb} + \text{Ta})$ being changed from 0.5 to 0.6 to 0.7 . It is noteworthy that there is a lack of any experimental values for the refractive indices for $\text{LiNb}_{1-x}\text{Ta}_x\text{O}_3$ materials in the literature. Xue *et al.*⁷ calculated the refractive indices of LNT for the crystal compositions of $x = 0.81$, 0.92 , and 0.97 , for which experimental values had already been reported. From their linear fit, the numerical dependence of n_o on the Ta content can be derived to be $n_o = 2.23 - 0.19x$, which gives 2.135 , 2.116 , and 2.097 for $x = 0.5$, 0.6 , and 0.7 , respectively (note that the equation gives the n_o value at $\lambda = 1064\text{ nm}$). Taking this into consideration, the three LNT films in Fig. 9(a) demonstrate somewhat lower refractive indices, which is believed to be due to the comparatively poor crystallinity of the films (FWHM = $0.32^{\circ}\text{--}0.35^{\circ}$). It should be mentioned that, in general, the refractive index is mainly influenced by the crystallinity and density of the film.^{37,38} Therefore the somewhat lower indices of the films suggest the presence of amorphous or not well-crystallized regions in the films in Fig. 9(a) grown at a relatively low growth rate ($R = 2\text{ ml/min}$), which is in agreement with the TEM observations by Shibata *et al.*³² and with Fig. 2.

The above suggestion agrees well with Fig. 9(b), where the refractive index for the LNT films ($x = 0.5$) is much improved, when their (006) rocking curve FWHM is decreased from 0.47° to 0.35° and finally to 0.19° . Note that the film with the narrowest FWHM demonstrates quite good optical quality, i.e., $n = 2.13$ at $\lambda = 800\text{ nm}$, which is very near the value of 2.135 calculated by Xue *et al.*⁷ for LNT at $x = 0.5$.

V. CONCLUSIONS

Highly c -axis oriented $\text{LiNb}_{1-x}\text{Ta}_x\text{O}_3$ films with high crystalline and epitaxial quality have been fabricated on as-received (001) sapphire substrates over the entire $0 \leq x \leq 1$ range using radio frequency thermal plasma in a soft $\text{O}_2\text{--Ar}$

vacuum of 150 Torr. The film properties have been shown to be strongly governed by the process parameters, i.e., substrate temperature and surface, growth rate, and precursor metal concentrations. The films were grown in the growth rate range of approximately 20–500 nm/min, although they demonstrated the best crystalline and epitaxial qualities at 180–380 nm/min, which seem to evolve even from the very early film nucleation and growth stages. Further research is needed to clarify in detail the nucleation and coalescence mechanisms on the sapphire surface. The x-ray diffraction revealed the high *c*-axis orientation of the films grown at optimal conditions and showed their good crystallinity. The 170–200-nm-thick films deposited under optimal growth conditions showed (006) rocking curve FWHM width down to 0.12° and achieved the (006) orientation close to 100%. They were in compression along the ⟨001⟩ direction and in extension in the (001) plane. No evidence of cracking was detected for films as thick as 200 nm, while thicker films of 400–600 nm often demonstrated cracking during cooling. The usage of precursors with higher metal concentrations was demonstrated to decrease the film surface roughness down to the root-mean-square value of about 5 nm. It is shown that the substrate surface condition is of great importance for the film orientation/crystallinity, namely, well-annealed (001) sapphire with very flat steps provides a lower active nucleation density and thus decreases the film (006) orientation degree. Finally, the evaluation of the optical properties (refractive index) confirmed the good quality and compositional control of the fabricated films. These results indicate that thermal plasma may be an attractive process for developing ferroelectric thin film devices in the future.

ACKNOWLEDGMENTS

The authors would like to thank J. Shibata for her TEM observations. The technical assistance of Y. Shimada and T. Yamaki during deposition experiments is also acknowledged. S.A.K. acknowledges the support of the Japan Society for the Promotion of Science (JSPS) during this work, which was financially supported by JSPS under the program “Research for the Future” (JSPS-RFTF Grant No. 97R15301).

¹L. M. Sheppard, *Ceram. Bull.* **71**, 85 (1992).

²D. K. Fork, F. Armani-Leplingard, and J. J. Kingston, *MRS Bull.* **21**, 53 (1996).

³R. S. Weis and T. K. Gaylord, *Appl. Phys. A: Mater. Sci. Process.* **A37**, 191 (1985).

⁴D. Kip, *Appl. Phys. B: Lasers Opt.* **B67**, 131 (1998).

⁵S. Y. Lee and R. S. Feigelson, *J. Cryst. Growth* **186**, 594 (1998).

⁶S. D. Cheng, C. H. Kam, Y. Zhou, X. Q. Han, W. X. Que, Y. L. Lam, Y. C. Chan, J. T. Oh, and W. S. Gan, *Thin Solid Films* **365**, 77 (2000).

⁷D. Xue, K. Betzler, and H. Hesse, *Solid State Commun.* **115**, 581 (2000).

⁸T. Kawaguchi, D.-H. Yoon, M. Minakata, Y. Okada, M. Imaeda, and T. Fukuda, *J. Cryst. Growth* **152**, 87 (1995).

⁹T. Kawaguchi, H. Kitayama, M. Imaeda, S. Ito, K. Kaigawa, T. Taniuchi, and T. Fukuda, *J. Cryst. Growth* **169**, 94 (1996).

¹⁰K. Kaigawa, T. Kawaguchi, M. Imaeda, H. Sakai, and T. Fukuda, *J. Cryst. Growth* **191**, 119 (1998).

¹¹T. N. Blanton and D. K. Chatterjee, *Thin Solid Films* **256**, 59 (1995).

¹²X. Lansiaux, E. Dogheche, D. Remiens, M. Guilloux-viry, A. Perrin, and P. Ruterana, *J. Appl. Phys.* **90**, 5274 (2001).

¹³R. A. Betts and C. W. Pitt, *Electron. Lett.* **21**, 960 (1985).

¹⁴Z. C. Wu, W. S. Hu, J. M. Liu, M. Wang, and Z. G. Liu, *Mater. Lett.* **34**, 332 (1998).

¹⁵W. S. Hu, Z. G. Liu, Z. C. Wu, J. M. Liu, X. Y. Chen, and D. Feng, *Appl. Surf. Sci.* **141**, 197 (1999).

¹⁶F. Veignant, M. Gandais, P. Aubert, and G. Garry, *J. Cryst. Growth* **196**, 141 (1999).

¹⁷Y. Kakehi, A. Okamoto, Y. Sakurai, Y. Nishikawa, T. Yotsuya, and S. Ogawa, *Appl. Surf. Sci.* **169–170**, 560 (2001).

¹⁸A. A. Wernberg, H. J. Gysling, and G. Braunstein, *J. Cryst. Growth* **140**, 57 (1994).

¹⁹R. S. Feigelson, *J. Cryst. Growth* **166**, 1 (1996).

²⁰S. Y. Lee and R. S. Feigelson, *J. Mater. Res.* **14**, 2662 (1999).

²¹S. Ono, T. Takeo, and S. Hirano, *J. Am. Ceram. Soc.* **79**, 1343 (1996).

²²K. Nashimoto, H. Moriyama, and E. Osakabe, *Jpn. J. Appl. Phys., Part 1* **35**, 4936 (1996).

²³V. Bouquet, E. R. Leite, E. Longo, J. A. Varela, M. Guilloux Viry, and A. Perrin, *J. Eur. Ceram. Soc.* **21**, 1521 (2001).

²⁴N. Yamaguchi, T. Hattori, K. Terashima, and T. Yoshida, *Thin Solid Films* **316**, 185 (1998).

²⁵Y. Takamura, K. Hayasaki, K. Terashima, and T. Yoshida, *J. Vac. Sci. Technol. B* **15**, 558 (1997).

²⁶Y. Takamura, N. Yamaguchi, K. Terashima, and T. Yoshida, *J. Appl. Phys.* **84**, 5084 (1998).

²⁷T. Majima, H. Yamamoto, S. A. Kulinich, and K. Terashima, *J. Cryst. Growth* **220**, 336 (2000).

²⁸S. A. Kulinich, J. Shibata, H. Yamamoto, Y. Shimada, K. Terashima, and T. Yoshida, *Appl. Surf. Sci.* **182**, 150 (2001).

²⁹H. Yamamoto, S. A. Kulinich, and K. Terashima, *Thin Solid Films* **390**, 1 (2001).

³⁰D. V. Shtansky, S. A. Kulinich, K. Terashima, T. Yoshida, and Y. Ikuhara, *J. Mater. Res.* **16**, 2271 (2001).

³¹S. A. Kulinich, H. Yamamoto, J. Shibata, K. Terashima, and T. Yoshida, *Thin Solid Films* **407**, 60 (2002).

³²J. Shibata, H. Yamamoto, S. A. Kulinich, T. Yamamoto, K. Terashima, T. Yoshida, and Y. Ikuhara, *Mater. Trans.* **43**, 1517 (2002).

³³M. Yoshimoto, T. Maeda, T. Ohnishi, and H. Koinuma, *Appl. Phys. Lett.* **67**, 2615 (1995).

³⁴G. H. Lee, M. Yoshimoto, and H. Koinuma, *Appl. Surf. Sci.* **127–129**, 393 (1998).

³⁵S. Adachi, *Phys. Rev. B* **35**, 7454 (1987).

³⁶G. Knuyt, C. Quaeys, J. D’Haen, and L. M. Stals, *Thin Solid Films* **258**, 159 (1995).

³⁷S. Ono, O. Böse, W. Unger, Y. Takeichi, and S. Hirano, *J. Am. Ceram. Soc.* **81**, 1749 (1998).

³⁸V. Bouquet, M. I. B. Bernardi, S. M. Zanetti, E. R. Leite, E. Longo, J. A. Varela, M. Guilloux Viry, and A. Perrin, *J. Mater. Res.* **15**, 2446 (2000).